Germline Deletion of *Igh* 3′ Regulatory Region Elements hs 5, 6, 7 (hs5–7) Affects B Cell-Specific Regulation, Rearrangement, and Insulation of the *Igh* Locus

Sabrina A. Volpi,*[,1] Jiyoti Verma-Gaur,[†] Rabih Hassan,* Zhongliang Ju,* Sergio Roa,*[,2] Sanjukta Chatterjee,* Uwe Werling,* Harry Hou, Jr.,* Britta Will,* Ulrich Steidl,* Matthew Scharff,* Winfried Edelman,* Ann J. Feeney,[†] and Barbara K. Birshtein*

Regulatory elements located within an ~28-kb region 3′ of the *Igh* gene cluster (3′ regulatory region) are required for class switch recombination and for high levels of IgH expression in plasma cells. We previously defined novel DNase I hypersensitive sites (hs) 5, 6, 7 immediately downstream of this region. The hs 5–7 region (hs5–7) contains a high density of binding sites for CCCTC-binding factor (CTCF), a zinc finger protein associated with mammalian insulator activity, and is an anchor for interactions with CTCF sites flanking the D_H region. To test the function of hs5–7, we generated mice with an 8-kb deletion encompassing all three hs elements. B cells from hs5–7 knockout (KO) (hs5–7KO) mice showed a modest increase in expression of the nearest downstream gene. In addition, *Igh* alleles in hs5–7KO mice were in a less contracted configuration compared with wild-type *Igh* alleles and showed a 2-fold increase in the usage of proximal V_H7183 gene families. Hs5–7KO mice were essentially indistinguishable from wild-type mice in B cell development, allelic regulation, class switch recombination, and chromosomal looping. We conclude that hs5–7, a high-density CTCF-binding region at the 3′ end of the *Igh* locus, impacts usage of V_H regions as far as 500 kb away.   *The Journal of Immunology*, 2012, 188: 2556–2566.

T he 3-Mb *Igh* locus undergoes DNA rearrangements and modifications in a highly regulated manner during B cell development. These include VDJ rearrangement, a combinatorial joining of variable (V), diversity (D), and joining (J) DNA segments to form a V region-coding exon; class switch recombination (CSR), which replaces the Ig Cμ H chain C region with one of the downstream C region exons (Cγ3, Cγ1, Cγ2b, Cγ2a, Cε, and Cα) that encode different effector functions; and somatic hypermutation (SHM), which introduces point mutations

in the Ig V region exon, resulting in increased affinity for Ag. Tight regulation of these DNA modifications is required to ensure proper functioning of the immune system and to prevent potentially oncogenic processes, derived from dsDNA breaks, from extending beyond the *Igh* locus.

Two main, long-distance *cis* regulators of the *Igh* locus are the intronic enhancer (Eμ) and the 3′ regulatory region (3′ RR). Eμ, located between J_H and Cμ, is composed of a 220-bp enhancer core and two flanking matrix-attachment regions. Analysis of various targeted and spontaneous knockouts (KOs) of Eμ revealed that it plays a pivotal role in aspects of VDJ recombination and allelic exclusion (1–6), and although necessary for IgH expression in early B cells (7, 8), it is dispensable for IgH expression in differentiated B cells (9–12).

The 3′ RR, located downstream of the *Igh* C region genes, consists of four DNaseI hypersensitive sites (hs), B lymphoid-specific enhancer elements (hs3a, hs1,2, hs3b, and hs4) (13, 14), which together are required for high levels of Ig transcription in plasma cells (12, 15–18) and class switching to all isotypes (19–21). CSR is essentially abrogated by the complete deletion of all four 3′ RR enhancers (20) and severely affected by the double deletion of hs3b and hs4 (19). Curiously, the activity of the 3′ RR can be conferred by several constellations of its elements, because individual KO of each of the 3′ RR enhancers (reviewed in Ref. 22), and, in fact, the double KO of hs3a and hs3b (23), have no deleterious effect. The various elements of the 3′ RR interact with each other and with target sites in the rearranged V region in plasma cells and with I/switch region sequences in resting B cells and B cells activated for germline transcription (GT) and CSR (23–26). These interactions are required for normal 3′ RR activity (24, 25).

We previously described additional hs elements downstream of hs4 (27): these novel sites (i.e., hs5, hs6, and hs7) display marks of open/active chromatin as early as the pro-B stage of B cell de-

velopment. The hs 5, 6, 7 region (hs5–7) (the focus of our study) contains a high density of binding sites for Pax5 and CCCTC-binding factor (CTCF): the latter is a zinc finger protein that has been extensively associated with all known mammalian insulator elements. In an in vitro cell culture assay, we showed that hs site 5 and hs site 7 exhibited insulator activity (27). Interestingly, chromatin immunoprecipitation and sequencing (ChIP-Seq) data showed that the density of CTCF sites in hs5–7 appears to be significantly greater than is typically seen in the genome (R. Casellas, personal communication). However, the contribution of hs5–7, with their high-density CTCF sites, to Igh regulation has not been assessed by the KO approach.

CTCF is predicted to exert its effects through tethering chromatin to subnuclear structures (28), promoting loop formation through contacts between two CTCF-bound sites (29), or facilitating long-range intrachromosomal and interchromosomal contacts (30–32). In addition to CTCF sites in hs5–7 (27), termed CTCF/3′ RR, CTCF-binding sites have been identified in pro- and pre-B cells throughout the Igh locus (i.e., two sites 3–5 kb upstream of DFL16.1, the most 5′ functional D_H gene, termed CTCF/DFL, and >60 binding sites within the V_H locus) (33–36). Recent studies showed chromosome conformation capture (3C) assay interactions in pre–pro-B cells and in pro-B cells between CTCF/3′ RR and CTCF/DFL, creating a loop that contains all of the D_H and J_H genes and both Eμ and the 3′ RR (35, 37). A knockdown of CTCF reduced the extent of these interactions and reduced V_H locus contraction (35). Mutations or deletion of the CTCF/DFL sites revealed a profound effect on VDJ recombination (38). Interactions among CTCF sites located throughout the V_H region could account for multiloop three-dimensional (3D) rosette-like structures previously predicted (39). Interestingly, deficiency of several proteins, including Ezh2, YY1, Ikaros, and Pax5 (with multiple binding sites in hs5–7), has also been associated with a lack of locus contraction and consequent impairment of distal V_H rearrangements (40–43).

To test the hypothesis that hs5–7, with its high density of CTCF/Pax5 sites, functions in VDJ joining and in Igh regulation at multiple stages of B cell development, we generated an hs5–7KO mouse line. Analysis of these mice revealed the impact of the deletion of hs5–7 within the context of an otherwise intact 3′ RR region. We found effects on VDJ rearrangement, Igh locus compaction, and Igh locus insulation.

Materials and Methods

Generation of hs5–7KO mice

An hs5–7-targeting vector was designed using the BD In-Fusion PCR cloning kit (catalog no. 631774). Briefly, the 8-kb genomic fragment encompassing hs5–7 was replaced with a neomycin resistance gene (pgk-Neo^R) flanked by loxP sites. PCR primers were designed to amplify 5′ (1891 bp) and 3′ (4599 bp) arms from bacterial artificial chromosome (BAC)199 M11 DNA (129Sv) (GenBank accession no. AF450245; http://www.ncbi.nlm.nih.gov/genbank/). The two arms and the linearized cloning vector provided by the BD In-Fusion PCR cloning kit (pDNA-dual cloning vector) were combined in a BD In-Fusion cloning reaction, according to the manufacturer's protocol, to create a new vector of 11,357 bp containing a unique BstB1 site. The Hygro/Neo cassette (3.8 kb) was inserted at the BstB1 site using a repeat of the BD In-Fusion cloning reaction, resulting in the final 15,390-bp, hs5–7-targeting vector. WW6 embryonic stem (ES) cells containing one 129Sv IgH allele and one C57BL/6 IgH allele (44) were transfected with the SalI linearized targeting vector by electroporation, and targeted cells were selected by resistance to G418. Southern blot analysis with probes 5′ and 3′ of the construct and PCR analysis identified 1 of 452 clones correctly targeted for the endogenous replacement of hs5–7 by the Neo^R cassette. The correctly targeted ES clone was injected into C57BL/6 blastocysts, which were introduced into pseudopregnant mice, and the resulting chimeras were mated with C57BL/6 animals. Germline transmission in heterozygous mutant mice was assessed by coat color, and

the presence of targeted alleles was confirmed by Southern blot and PCR analysis. Southern analysis, using 10–15 μg genomic DNA, with a probe 5′ of the construct (Probe X, in hs4, Fig. 1, Supplemental Fig. 1) distinguished the wild-type (WT) allele (4.7 kb) from the hs5–7 Neo^R-replaced allele (3.2 kb) when DNA was digested with 200–300 U EcoRI and NdeI. Similarly, a probe 3′ of the construct (Probe Y, in the 48-kb region, Fig. 1, Supplemental Fig. 1) distinguished the WT allele (13.3 kb) from the hs5–7 Neo^R-replaced allele (10.6 kb) when DNA was digested with SpeI. Mutant mice were mated with EIIa-Cre–transgenic mice to delete the Neo^R gene. We initially compared mice containing the Neo^R gene with mice containing a clean deletion of hs5–7. Because no differences were seen between these mice, we focused our experiments on mice in which hs5–7 were cleanly deleted (i.e., hs5–7KO mice). Mice were backcrossed to the F10 generation. Progeny were checked by PCR analysis. PCR primers designed in the 5′ and 3′ arms (primers 1 and 2, Fig. 1) generated a 566-bp product in cleanly deleted hs5–7 alleles. PCRs for hs site 5 (517 bp), hs site 6 (325 bp), and hs site 7 (594 bp) were also done to confirm their absence in homozygous mice (Supplemental Fig. 1). Genotyping was always done twice, and breeding revealed Mendelian transmission. All primers are listed in Supplemental Table I.

WT mice controls

Mutant mice contained the hs5–7 targeted deletion on 129Sv alleles and were backcrossed onto C57BL/6 mice. Therefore, homozygous hs5–7KO mice have Igh alleles from the 129Sv strain, allotype (a), whereas WT littermates have normal Igh alleles from the C57BL/6 strain, allotype (b). To control for biological differences that may be attributed to strain (45), we used WT mice controls from Jackson Laboratories that contained 129Sv Igh alleles on a C57BL/6 background (B6.Cg-IgH^a Thy1^a Gpi$^{a/}$J; stock no. 001317) (referred to in this article as B6.IgH^a), as well as WT C57BL/6 littermates. As a control for heterozygous mutant mice, we used a Jackson Laboratory WT F1 mouse from a C57BL/6 and 129Sv cross (B6129SF1/J; stock no. 101043). Specifically for analysis of locus contraction and quantitative analyses of VDJ joining, μMT mice (B6.129S2-Ighm) (containing IgH^a alleles and an inactivating mutation of the membrane exon of the μ chain gene on the C57BL/6 background) were used as the WT control. All mice were used in accordance with institutional review board approval from Albert Einstein College of Medicine.

Isolation of B cells from bone marrow and spleen

Cells were isolated from femurs and tibias of 6–8-wk-old mice (for examination of bone marrow [BM] populations) or 4–6-wk-old mice (for VDJ joining assays) by flushing bones with PBS supplemented with 10% FBS. Cells were washed twice with PBS and 3% FBS and resuspended in 3 ml RBC lysis buffer (158902; QIAGEN) for 2 min at room temperature. The cell suspension was preblocked with 0.2 μg/10^6 cells of rat anti-mouse FcγIII/IIR Ab (553142; BD Pharmingen) for 40 min on ice. Cells were washed and resuspended in PBS and 3% FBS. BM cells were stained and sorted on the DakoCytomation MoFlo for the pro-B (IgM$^-$, CD19$^+$, cKit$^+$), pre-B (IgM$^-$, CD19$^+$, CD25$^+$), immature early (IgD$^-$, CD19$^+$, IgM^{lo}), and immature late (IgD$^-$, CD19$^+$, IgM^{hi}) stages of B cell development. Flow cytometric analysis was performed using 1×10^6 cells in a total volume of 100 μl. Cells were stained with selected Abs (Supplemental Table I) for 45–60 min at 4°C and analyzed with the Becton Dickinson FACScan or FACSCalibur.

Splenic B cells were isolated from 6–8-wk-old mice. Single-cell suspensions were generated, and RBCs were lysed. Cells were labeled with CD43 MACS MicroBeads (130-049-801; Miltenyi Biotec), according to the manufacturer's protocol, and CD43$^+$-activated B cells and non-B cells were depleted from total splenocytes by negative selection using MS MACS Separation columns (130-042-201; Miltenyi Biotec). Negative selection of resting mature B cells resulted in a purity >95%, as evaluated by FACS analysis of CD43$^-$, B220$^+$, and CD3ε$^-$ cells.

3D-fluorescence in situ hybridization

3D-fluorescence in situ hybridization (FISH) was performed, as previously described (35). Briefly, WT (μMT) and hs5–7KO pro B cells were cultured for a week in the presence of IL-7 and stem cell factor. Cells adhering to polylysine-coated slides or coverslips were fixed in paraformaldehyde and then permeabilized and hybridized with labeled BACs. BACs were purified with Macherey-Nagel Nucleobond midi kits and labeled by nick translation using Roche nick translation mix and Invitrogen Alexa Fluor deoxyuridine triphosphate. BAC CT7-167C1 ("7183"), which spans 31 kb of the proximal V_H region, including seven V_H genes plus 77 kb between these genes and DFL16.1, was labeled with Alexa Fluor 568. BAC RP24-189H12 ("J558") hybridizes just upstream of the V_H locus and was labeled with Alexa Fluor 488. 3D image stacks were captured with a BioRad-Zeiss radiance confocal 2100 microscope system located at the Scripps Research

Institute Core Microscopy Facility. Images were captured with a $100\times$ lens at 0.3-μm Z steps. The image stacks were analyzed with Imaris 7.1.1 software. Only cells containing signals from both *IgH* alleles were evaluated. The differences between the WT (μMT) and hs5–7KO samples were analyzed using a two-tailed *t* test.

Assays for $V_H DJ_H$ and DJ_H rearrangements

Genomic DNA was isolated from BM cell populations by phenol chloroform extraction, and PCR reactions were performed on serial 3-fold dilutions to detect D-to-J_H and V_H-to-DJ_H rearrangements (4). PCR products were detected via Southern blot hybridization using an oligonucleotide probe specific to the J_H4 region. Genomic DNA input was normalized by PCR amplification of hs4. Primers and probe sequences were generated from those previously published (4). In other experiments, genomic DNA was isolated using QIAamp DNA mini kit (QIAGEN) from pro-B cells grown in short-term culture, as previously described (46). The level of V_H7183 and V_HJ558 recombination was determined by TaqMan PCR reaction (TaqMan Universal PCR master mix II; Applied Biosystems) using forward primers and TaqMan probes located in V_H7183 and V_HJ558 and a reverse primer in J_H1 and J_H4. Data were normalized with TaqMan PCR of the Eμ region, because this region remains unaltered by VDJ rearrangement. The primer sequences and TaqMan probe sequences are given in Supplemental Table I.

In vitro switching assays

A total of $0.5–1 \times 10^6$ splenic B cells/ml was stimulated with 25 μg/ml LPS (*E. coli* E:55, 437625; Calbiochem) for switching to IgG3 and IgG2b; 25 μg/ml LPS + 25 ng/ml IL-4 (214-14; PeproTech) for switching to IgG1; and 25 μg/ml LPS + 100 ng IFN-γ (315-05; PeproTech) + 10 ng/ml BAFF (215-15; PeproTech) for switching to IgG2a in complete RPMI media. IgG1, IgG2b, IgG2a, and IgG3 germline transcripts were analyzed after stimulation of splenic B cells for 48 h. Briefly, TRIzol was used to isolate RNA, followed by chloroform extraction, isopropanol precipitation, and cDNA synthesis using Superscript III First-Strand (18080-051; Invitrogen). GT was assessed by RT-PCR, as previously described (47, 48), using calreticulin as a normalizing control. After 96 h of stimulation, B cells bearing surface IgM and IgG were analyzed by flow cytometry, as described above, using the Becton-Dickinson FACSCalibur or FACScan and FlowJo software (Tree Star). Cell suspensions were preblocked with 0.2 μg/10^6 cells of rat anti-mouse FcγIII/IIR Ab (553142; BD Pharmingen) for 40 min on ice. Refer to Supplemental Table I for a list of all Abs.

Expression of downstream non-IgH genes

Total RNA was extracted from ~10^7 WT and hs5–7KO splenic B cells at 0, 48, and 96 h after LPS+/−IL-4 stimulation using a standard TRIzol, chloroform, and isopropanol-precipitation method. A total of 2–4 μg RNA was treated with RQ1 RNase-free DNase, and cDNA was prepared using Superscript III First-Strand kit (18080-051; Invitrogen), as per the manufacturer's protocol. Expression levels of downstream non-*Igh* genes were examined in triplicate via real-time PCR, normalizing to the GAPDH housekeeping gene. Analysis of gene expression levels was performed using the $2^{-\Delta\Delta CT}$ method, as described (49). Briefly, using Excel, the normalized ΔCT value of each downstream gene was calculated using the formula: ΔCT = power (2, average CT of normalizing gene − average CT of gene of interest). The SD for ΔCT was next calculated by: SD ΔCT = absolute value [power(2, average CT normalizing gene + SD normalizing gene − average CT gene of interest − SD gene of interest) − power (2, average CT normalizing gene − average CT gene of interest)]. CT values are converted with power formulas because a difference in CT of (*n*) corresponds to a difference at the RNA level of 2^n. The normalized ΔCT was calculated for each of the downstream genes in WT and hs5–7KO cells and plotted on the *y*-axis for comparison. Fold enrichment of expression of downstream genes in hs5–7KO mice compared with WT mice was calculated as follows: fold enrichment = ΔCT (normalized) of KO/ΔCT (normalized) of WT. A value > 1 indicates that KO cells are expressing downstream genes at higher levels compared with WT controls. The SD for fold enrichment was calculated as follows: sqrt ((SD of ΔCT of KO/ΔCT of KO)^2 + (SD of ΔCT of WT/ΔCT of WT)^2) $\times$ fold enrichment. Primers are listed in Supplemental Table I.

SHM assays

Three WT and three hs5–7KO mice were immunized with 5×10^8 SRBCs by i.p. injection. Twelve days later, spleens were isolated, splenocytes were depleted of RBCs, and germinal center B cells (B220$^+$, GL7$^+$, and Fas$^+$) were sorted. DNA was extracted from the sorted cells, and the J_H2–J_H4 intron region was amplified (primers are listed in Supplemental Table I).

The 1.5-kb PCR product was gel extracted, cloned (Zero Blunt Topo PCR Cloning Kit for Sequencing, catalog no. 45-00310; Invitrogen) and sequenced, as previously described (50, 51). Alignment and analysis of unique mutations were done using Seqman 5.07 (DNASTAR) and SHMTool (http://scb.aecom.yu.edu/shmtool) (52). As consensus sequences, GenBank NT_166318.1 (nucleotides 25620784–25620092, C57BL/6) and NT_114985.2 (nucleotides 1206584–1207483, 129Sv) for the J_H2–J_H4 region were used. The presence of A > T and W<u>A</u> > <u>T</u>W (where W = A/T) bias in mutation data was used for quality assessment to rule out any artifacts in mutation data that may have arisen through PCR (51, 53). The site in hotspot motifs that was analyzed for mutation is underlined.

Chromosome conformation capture assay

The 3C assay was performed with WT and hs5–7KO resting splenic B cells or after 48 h of stimulation with LPS+/−IL-4, as described previously (24). Ligated DNA samples were analyzed by PCR using 100 ng DNA. Gel pictures were captured by Gene Snap Software and analyzed by Gene Tools Software (Syngene Gene genius BioImaging System). To correct for differences in amplification efficiency between different primer sets, an equimolar mixture of BACs (containing all sequences of interests) and two calreticulin fragments that contain the selected HindIII restriction sites were used as a control template. Experiments (3C) were performed on two independent cell preparations using three independent PCR reactions. 3C analysis to examine the interaction of the DFL/CTCF and 3′ RR regions in pro-B cell samples from μMT and hs5–7KO mice was performed, as described previously (35), on two independent cell preparations. All primers used are in Supplemental Table I.

Results

Generation of hs5–7KO mice

To determine the role of hs5, hs6, and hs7 in regulating the *Igh* locus, we generated a mouse KO model. As described in *Materials and Methods* (Fig. 1, Supplemental Fig. 1), we replaced an 8-kb fragment containing hs5–7 with a pgk-Neo^R gene flanked by loxP sites. Somatic chimeras were bred to EIIa-cre–transgenic mice to obtain heterozygous mice in which the Neo^R gene was deleted via loxP/Cre-mediated recombination. The heterozygous mice were further bred to generate the homozygous hs5–7$^{-/-}$ line, which we refer to as hs5–7KO. Progeny were checked by Southern blot (Supplemental Fig. 1A) or PCR analysis (Supplemental Fig. 1B). Mice were backcrossed to the F10 generation.

B cell and lymphoid tissue development

There were no significant histological differences in WT and hs5–7KO mice in thymus, submandibular salivary gland and lymph node, mesenteric lymph node, small intestine, spleen, and Peyer's patches, as documented by the Einstein histopathology facility. Percentages of B cells and T cells in spleens, as well as of macrophages in BM, were similar in WT and hs5–7KO mice (Fig. 2A–D). FACS analysis of six of seven independent experiments, each of which monitored three to five mice, showed that percentages of BM pro-B, pre-B, and B cells were similar in WT and hs5–7KO mice (Fig. 2E, Supplemental Fig. 2). However, in one analysis, a group of five hs5–7KO mice showed a greater percentage of pro-B (2.7-fold), pre-B (3.5-fold), and immature early B cells (3.1-fold) compared with WT mice, with no apparent alterations in a later (immature late) B cell stage (Supplemental Fig. 2). No differences were observed in hematopoietic stem cells or lymphoid progenitor cells (Fig. 2F). We conclude that deletion of hs5–7 does not grossly affect the outcome of lymphoid tissue development.

Expression of downstream non-Igh genes as measure of hs5–7 in vivo insulator activity

Based on the multiple CTCF sites within hs5–7 (27), we proposed that hs5–7 insulated *Igh* 3′ RR enhancers from activating nearby downstream non-*Igh* genes (located in order): *Igh*: *Tmem121* (*Hole*), *4930427A07 Rik1* (a pseudogene referred to as *Rik1*
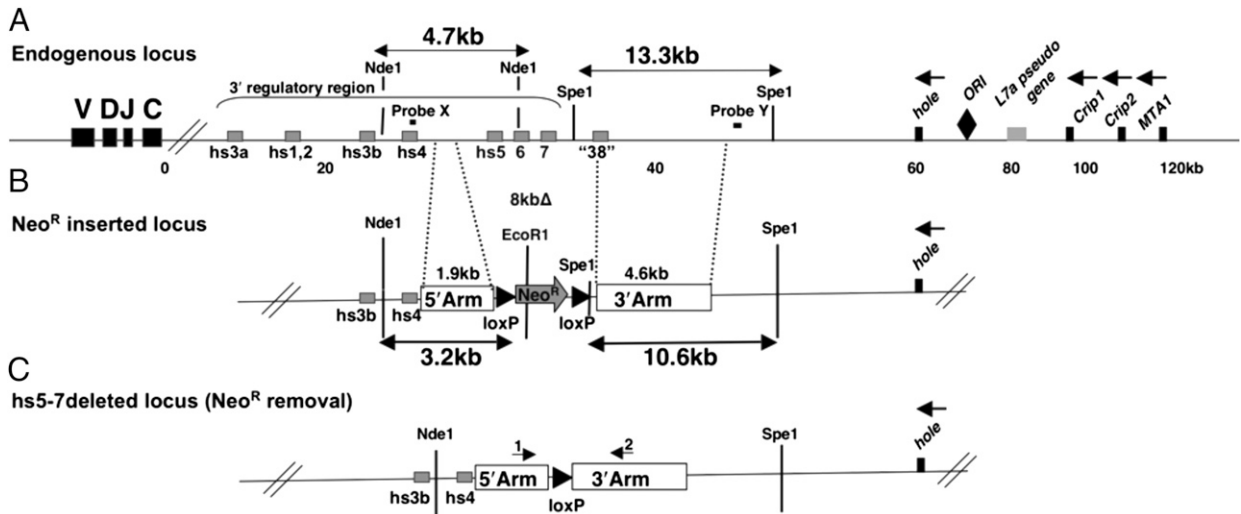
FIGURE 1. Targeting of the IgH (*Igh*) hs5–7 elements for genomic deletion. (**A**) Map of the mouse WT H chain 3′ RR in context of upstream H chain genes and downstream non-*Igh* genes. The "38" downstream region is located immediately downstream of the 3′ deletion breakpoint (26). Locations refer to BAC199 M11 sequence (accession number: AF450245). Probes (X and Y), restriction enzyme sites, and fragments used in screening targeted ES clones are depicted. (**B**) Schematic of the locus in which Neo[R] replaces an 8-kb segment containing hs5–7. (**C**) Map of the hs5–7 locus after deletion of Neo[R] with Cre recombinase. Primers 1 and 2 were used for genotyping hs5–7KO mice. Southern and PCR analysis used in screening of targeted ES clones and genotyping of hs5–7KO mice are shown in Supplemental Fig. 1.

throughout the article), and *Mta1* (*Crip1* and *Crip2* were not quantitated.) To ensure that any differences seen in expression levels of downstream genes did not reflect differences in mouse strains, we compared hs5–7KO mice (129Sv *Igh* alleles on a C57BL/6 background) with C57BL/6 WT mice that similarly contained 129Sv *Igh* loci (B6.IgH[a], described in *Materials and Methods*).

B cells were isolated from spleens of WT and hs5–7KO mice at 0, 48, and 96 h after LPS stimulation. Real-time PCR analysis of RNA levels revealed a modest, albeit statistically significant, increase in expression of the nearest downstream gene, *Hole*, in hs5–7KO mice compared with WT mice in both resting B cells (1.7-fold enrichment [KO/WT]) and upon stimulation for switch-
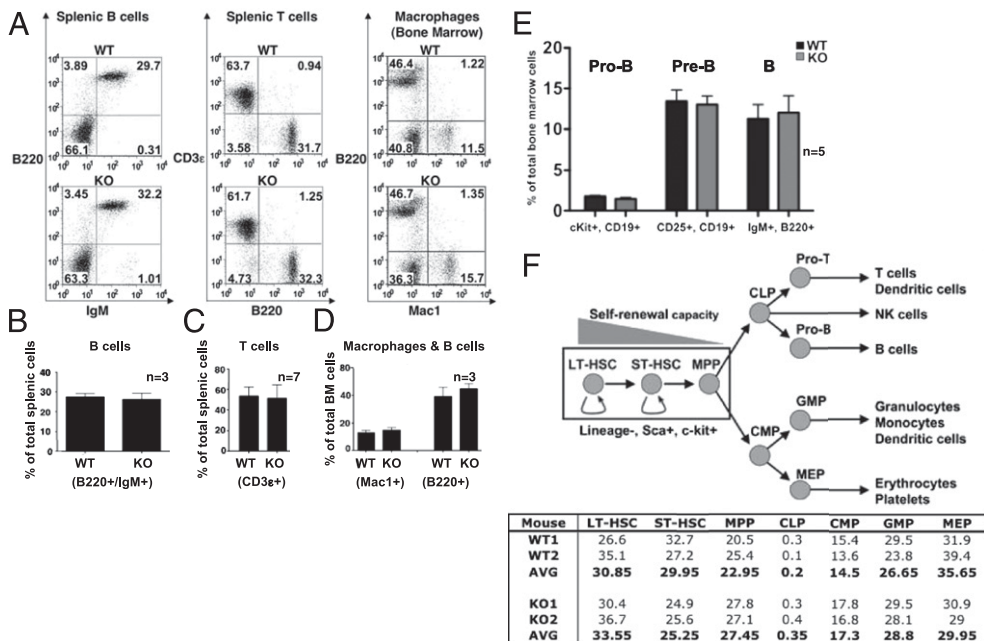

FIGURE 2. Flow cytometric analysis of B and non-B cells. BM and splenic cells of WT and hs5–7KO mice were stained with appropriate fluorescent Abs. (**A**) Splenic B cells in WT and hs5–7KO mice examined by staining with anti-B220 and anti-IgM (*left panels*). Percentages of splenic B and T cells were determined by staining with anti-B220 and anti-CD3ε (*middle panels*). Percentages of BM B cells and macrophages were determined by staining with anti-B220 and anti-Mac1 (*right panels*). Experiments were repeated three to seven times, each with three to five mice, and a representative experiment is shown. Averages are shown in (**B**)–(**D**). (B) Averages from three experiments showing anti-B220 and anti-IgM B cells. (C) Averages of seven experiments showing percentages of splenic T cells. (D) Averages of three experiments showing percentages of BM B cells and macrophages. (**E**) Stages of B cell development in BM cells. Total BM cells from three to five WT and hs5–7KO mice were stained with anti–c-Kit and anti-CD19 (pro-B), anti-CD25 and anti-CD19 (pre-B), and anti-IgM and anti-B220 (B cells). The averages from five experiments are shown. (**F**) Examination of hematopoietic stem cells and lymphoid progenitor cells from WT and hs5–7KO BM cells. Percentages of total BM cell populations from two WT and two hs5–7KO mice are shown.

ing (2.9- and 4.8-fold enrichment at 48 and 96 h, respectively). Although *Hole* expression was substantially decreased during switching, these mRNA levels were sufficient to be monitored by real-time PCR analysis. Expression levels of the next downstream gene, *Rik1*, tended toward a modest increase in resting cells (i.e., 2.3-fold enrichment); however, this was not statistically significant ($p > 0.05$), and *Mta1* levels remained unchanged (Fig. 3B, 3C), We conclude that hs5–7 modestly contribute to insulation of the *Hole* gene, which is located ~65 kb from the *Igh* locus; additional local insulation mechanisms of this and further-downstream genes likely exist.
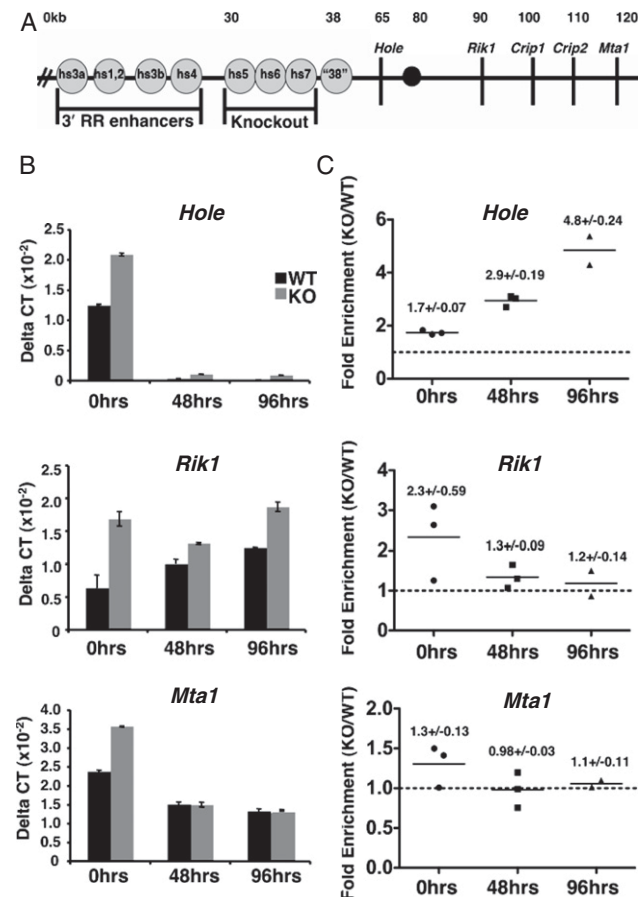

FIGURE 3. Effect of hs5–7KO on expression levels of downstream *Hole* (*Tmem121*), *Rik1*, and *Mta1* non-*Igh* genes. mRNA levels of downstream genes in resting B cells and B cells treated with LPS from WT and hs5–7KO mice for 48 and 96 h were analyzed in triplicate by real-time PCR and normalized to the GAPDH housekeeping gene. Three to five WT and hs5–7KO mice, 6–8 wk old, were used per experiment. (**A**) Schematic of the deleted area and location of downstream genes on BAC199M11. Filled circle identifies origin of replication for *Igh* C_H genes (66). (**B**) One of three experiments, analyzing expression levels over time for downstream genes in WT and hs5–7KO mice. The *y*-axis plots the ΔCT value, calculated as described in *Materials and Methods*. The ΔCT value normalizes expression of the tested downstream genes to GAPDH. (**C**) Fold enrichment (KO/WT) from all three experiments. A value >1 is indicative of greater expression in hs5–7KO mice. In one experiment, starting B cells were divided into two populations and subsequently examined independently, with the results averaged into a single number. An unpaired two-tailed *t* test analyzing expression levels between WT and hs5–7KO mice revealed *p* values < 0.05 for *Hole* expression (0 h: $p = 0.003$; 48 h: $p = 0.001$; 96 h: $p = 0.003$). All other values were >0.05.

Long-range looping, locus contraction, and VDJ rearrangement in hs5–7KO mice

Our recent experiments (35) showed long-range interactions between CTCF sites in the hs5–7 region of the 3′ RR (3′ RR/CTCF) and two CTCF sites located upstream of the most 5′ D_H gene, DFL16.1 (DFL/CTCF). Short hairpin RNA knockdown of CTCF resulted in reduction of these loop interactions. In this study, we tested the effect of deletion of hs5–7 on the 3′ RR/CTCF–DFL/CTCF interactions by 3C. A primer for this region (SD180), used in our previous study to analyze these interactions (35) (Fig. 4A), was not deleted in hs5–7KO mice. Using this primer, we found that 3C interaction between residual sequences upstream of hs5 and DFL/CTCF was greatly reduced in hs5–7KO pro-B cells, as anticipated (Fig. 4B).

In addition, we previously reported (35) that knockdown of CTCF in pro-B cells resulted in an increase in spatial distance between distal and proximal V_H gene families, as assayed by 3D-FISH. To determine whether deletion of the 3′ RR/CTCF region, which contains an especially high density of CTCF sites, had an effect on this interval, we compared spatial distances between V_H gene families in pro-B cells from WT and hs5–7KO mice. Using 3D-FISH (Fig. 4A, 4C), we found that the distance between distal V_HJ558 and proximal V_H7183 gene families in hs5–7KO pro-B cells was greater than in pro-B cells from normal μMT mice ($p = 0.0001$) (Fig. 4C), although it was less than observed in the CTCF knockdown pro-B cells (35).

Locus contraction has been associated with acquisition of usage of distal V_H gene families in VDJ rearrangements (40). In fact, real-time PCR assays with TaqMan probes revealed no difference in rearrangement of the distal V_HJ558 genes. However, there was an ~2-fold increase in usage of proximal V_H7183 family in pro-B cells from hs5–7KO mice compared with μMT control pro-B cells (Fig. 4D).

These observations were extended by a PCR-based approach to assay for D_H-to-J_H and V_H-to-DJ_H rearrangements in BM early B cell populations. Products were detected with Southern blot analysis using a radiolabeled probe for the J_H4 segment (Fig. 4A, 4E). Although this assay system was not sensitive enough to detect the increased usage of V_H7183 genes, we found that all D_H and V_H families assayed were used for VDJ joining. In addition, we detected increased amounts of the rearrangement of DQ52 to the J_H3 region in hs5–7KO mice (Fig. 4E). Together, these results suggest that hs5–7 participates in the regulation of the contraction and usage of proximal V gene segments during V(D)J recombination.

IgM allotypic expression

Expressed IgM alleles can be distinguished in hs5–7 heterozygous mice using Abs specific to the targeted "a" allotype (129Sv) or the "b" allotype (C57BL/6). Total splenocytes (and BM cells; data not shown) from WT (B6129SF1/J) and hs5–7 heterozygous KO mice expressed either surface IgM[a] or IgM[b] but not both (Fig. 5A). Furthermore, the mutant 129Sv allele (IgM[a]) in heterozygous mice is expressed in serum at levels similar to the 129Sv allele in WT mice (Fig. 5B). We conclude that deletion of hs5–7 does not decrease efficiency of functional VDJ rearrangement, even in competition with the WT allele, nor does hs5–7 deletion breach allelic exclusion. In addition, there are no significant effects on levels of allelic expression, as revealed by IgM surface expression, or serum IgM levels.

Somatic hypermutation

To determine whether deletion of hs5–7 affected SHM, we immunized three hs5–7KO mice and three WT littermates with SRBCs
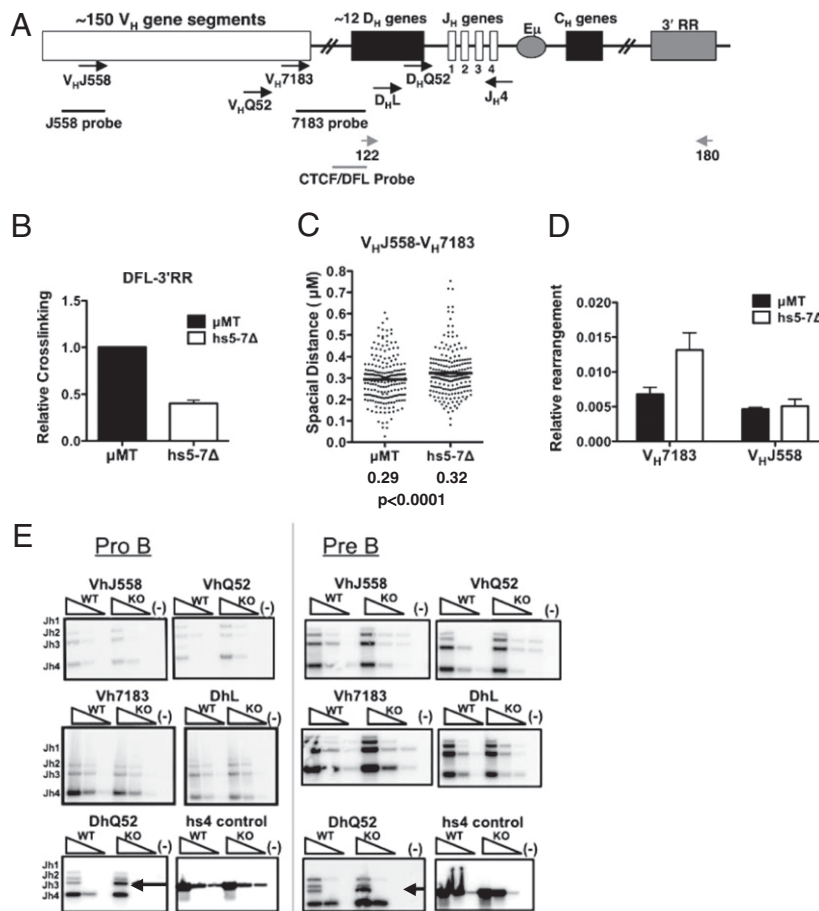
FIGURE 4. Deletion of hs5–7 affects *Igh* locus contraction and VDJ joining. (**A**) Schematic indicating location of the BAC probes used in FISH to measure locus contraction, primers used in rearrangement assays (both shown in black), and probes and primers for 3C analysis of CTCF/DFL-CTCF/3′ RR interactions (gray). (**B**) 3C data showing the decrease in CTCF/DFL–CTCF/3′ RR interactions in hs5–7KO mice. (**C**) *Igh* locus contraction, as measured by two-color 3D DNA FISH using probes in the V_H region. One BAC probe was derived from upstream of the V_H J558 gene segments, and the second probe included the proximal approximately seven V_H genes, extending 3′ ~70 kb toward the DFL gene segments. Two hundred WT (μMT) and 202 hs5–7KO alleles were analyzed. μMT mice were used to control for any differences due to strain. Results showed that significantly more hs5–7KO alleles were in a less contracted configuration ($p < 0.0001$). (**D** and **E**) Analysis of DJ and VDJ joining in hs5–7KO mice. (D) Increased usage of proximal V_H7183 genes in hs5–7KO mice. V_H–DJ_H rearrangements assayed using real-time PCR with TaqMan probes for the V_H7183 and V_HJ558 rearrangements. Hs5–7KO mice have a slight bias toward proximal V_H7183 rearrangements compared with WT (μMT) controls. (E) Genomic DNA from sorted pro-B and pre-B cell populations from WT (B6.IgH^a) and hs5–7KO mice were subjected to PCR amplification of D_H-to-J_H and V_H-to-DJ_H rearrangements. PCR reactions were performed on 3-fold serially diluted DNA, and products were detected via Southern blot using a probe specific to the J_H4 region. DNA input was normalized to amplification of the hs4 enhancer. Southern blot analysis of rearrangements in sorted pro- or pre-B DNA, using either a V_H or D_H forward primer with a J_H4 reverse primer, shows the use of all V and D families in VDJ and DJ joining in WT and hs5–7KO mice. Arrow indicates the increase in J_H3 usage observed in KO DNA. A similar increase in J_H3 usage was observed in immature early and late stages of B cell development (data not shown).

and 12 d later sorted for B220$^+$/GL7$^+$/Fas$^+$ (germinal center) splenic B cells, known to be induced by this Ag (54). Because SHM extends into the J-C introns downstream of all rearranged V_H genes (55), we quantified mutations in a 555-bp region at the 5′ end of the PCR product within the J_H2–J_H4 intronic region. Analysis of 56 sequences from three WT mice and 43 sequences from three hs5–7KO mice showed that the mutation spectra were identical, with one exceptional sequence from WT mice that had >10 mutations. Analysis of the entirety of the data showed that the overall mutation frequency was slightly decreased in hs5–7KO mice ($p = 0.05$) (Fig. 6); KO mice showed a tendency toward reduced mutation frequency at the A:T bp, G:C bp, and Polη hotspots (W<u>A</u>/T<u>W</u>), but not at the AID hotspots (WR<u>C</u>/<u>G</u>YW; underlined base was analyzed for mutation). However, because the single sequence with >10 mutations was derived from WT mice, these conclusions are potentially fortuitously biased, and we conclude that hs5–7 contribute modestly, if at all, to SHM.

CSR in mutant mice

There were no differences in GT of IgG3, IgG1, IgG2b, and IgG2a in B cells from hs5–7KO mice and WT mice stimulated in culture when examined by semiquantitative RT-PCR (Fig. 7A). FACS analysis of cells stimulated ex vivo to undergo CSR showed no differences in CSR for any isotype other than a modest, but significant, increase in IgG1$^+$ cells ($p = 0.02$, Fig. 7B). Thus, we conclude that, except for the small increase in IgG1, the deletion of hs5–7 has no effect on CSR, as measured in cultured cells.

Long-range interactions involving 3′ RR in resting and LPS-activated B cells

In resting B cells and plasma cells, the 3′ RR (including hs5–7) is in close proximity to the expressed VDJ gene and/or Eμ, resulting in chromosomal loops (24, 25). These V_H and/or Eμ interactions with the 3′ RR are necessary for maintaining normal IgH expression in plasma cells (24). Upon B cell activation, recruitment
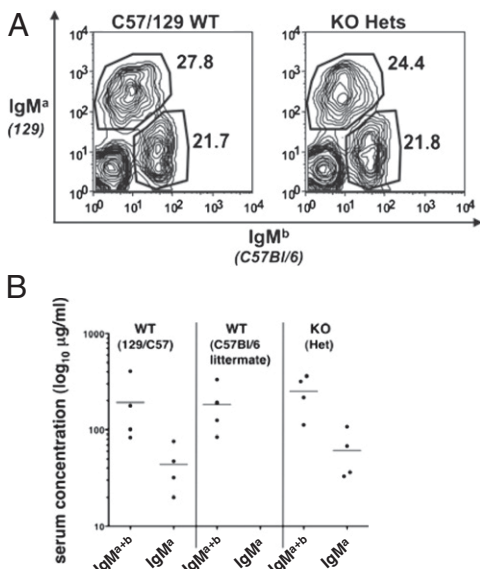
FIGURE 5. IgM allotypic expression in WT and heterozygous hs5–7KO mice. (**A**) Flow cytometry profiles of total splenocytes stained with anti-IgM^a (specific to the 129Sv allotype) and anti-IgM^b (specific to the C57BL/6 allotype). WT mice are a F1 cross of 129Sv and C57BL/6. This is a representative of three experiments with similar findings. (**B**) ELISA analysis of WT and heterozygous mice serum from 6–8-wk-old mice using anti-IgM (recognizing both "a" and "b" allotypes) and anti-IgM^a (recognizing only the "a" allotype.

of I region promoters to these 3′ RR–Eμ loops is enhanced in a cytokine-dependent manner and is essential for GT prior to CSR (23, 25, 26).

3C analysis of resting B cells showed no differences between WT and hs5–7KO mice in cross-linking efficiency between Eμ

(or J$_H$3) and 3′ enhancers (i.e., hs3a, hs1,2, and hs4). These intrachromosomal interactions are cell type specific, because little amplification was observed in CD43$^+$ splenic T cells (Fig. 8A, 8B). Similarly, no differences between cross-linking frequency of the 3′ RR with I regions (Fig. 8C) or Eμ (Fig. 8D) or interactions among the 3′ RR segments themselves (Fig. 8E) were observed in resting B cells or cells activated by LPS+/−IL-4 originating in WT and hs5–7KO. We tested the prediction that, in the absence of CTCF sites in hs5–7, new loops between 3′ RR enhancers could form with the promoters of downstream genes. However, no loops between hs3a and the nearest downstream gene, *Hole*, were acquired in the hs5–7KO mice during stimulation (Fig. 8E).

Discussion

Effect of hs5–7 on CSR

The 3′ RR can be subdivided into an upstream enhancer-containing region and downstream hs5–7, CTCF/Pax5-rich island. Functionally, the enhancer-containing region was shown to be essential for GT and CSR (20, 56), as well as expression of high levels of secreted Igs in plasma cells (20), and it may contribute to normal levels of SHM (21). These processes involve loop formation, executed by interactions among the 3′ regulators themselves, including hs5–7, and between the 3′ RR and target I regions and V$_H$ promoters (20, 23–26). Analysis of hs5–7KO mice suggests that hs5–7 may also contribute to CSR regulation, based on a small, but significant, increase in the numbers of B cells from hs5–7KO mice that switch to IgG1 when stimulated ex vivo with LPS + IL-4. We predicted that hs5–7 might modulate the enhancer-containing segment of the 3′ RR, but we saw no differences within the sensitivity of the 3C assays in interactions between 3′ RR enhancers with anchors Eμ or J$_H$3, and Iγ1 or Iγ3, in hs5–7KO B cells stimulated to switch, or among the enhancers themselves. These observations are consistent

FIGURE 6. SHM in the J$_H$2–J$_H$4 region of the IgH locus in WT and hs5–7KO mice. Germinal center B cell DNA was isolated from B220$^+$, GL7$^+$, and Fas$^+$ splenocytes of 6–8-wk-old mice immunized with SRBCs 12 d prior to sorting. (**A**) Analysis of unique mutation frequencies corrected for base composition. All mutation frequencies were calculated according to the standardization method suggested in SHMTool (52). N = number of mice assayed. No values were found to be significantly different using a two-tailed χ^2 test. (**B**) WT and hs5–7KO pie charts showing numbers of sequences analyzed (at the center), the percentages of sequences containing 0, 1–3, 4–10, and >10 mutations (at the perimeter and proportional to the area in each slice), and overall mutation frequency. It should be noted that the single sequence containing >10 mutations was obtained from WT mice, potentially impacting unduly on the significance ($p = 0.05$) of these data. (**C**) The spectrum of base substitutions presented as absolute counts and as frequencies of mutation ($\times 10^{-3}$ mutations/base) corrected for base composition. The site in hotspot motifs that was analyzed for mutation is underlined. W = A/T, R = A/G, and Y = C/T.
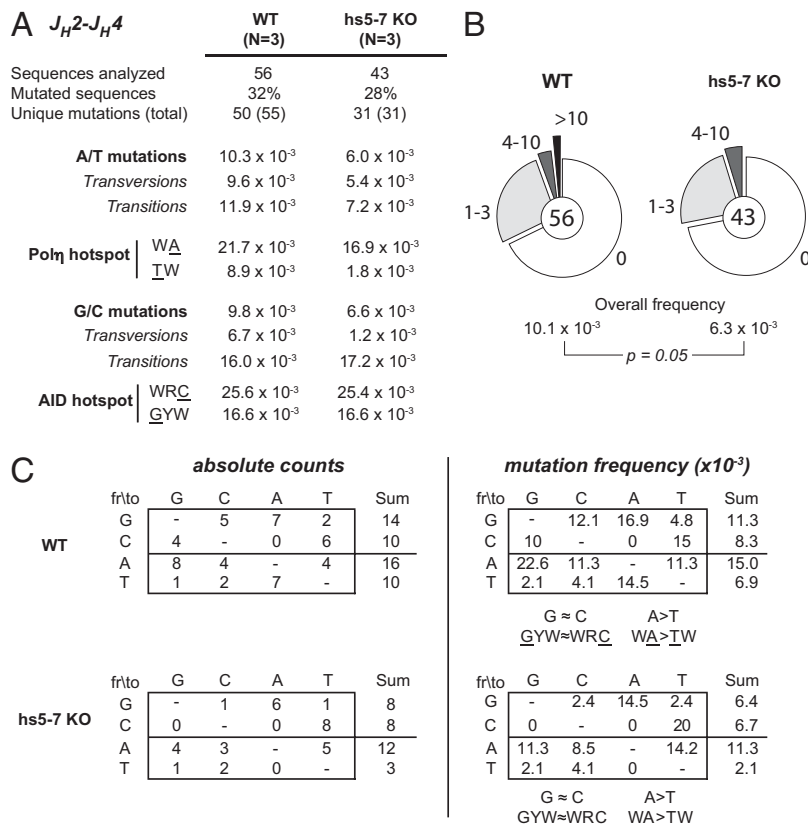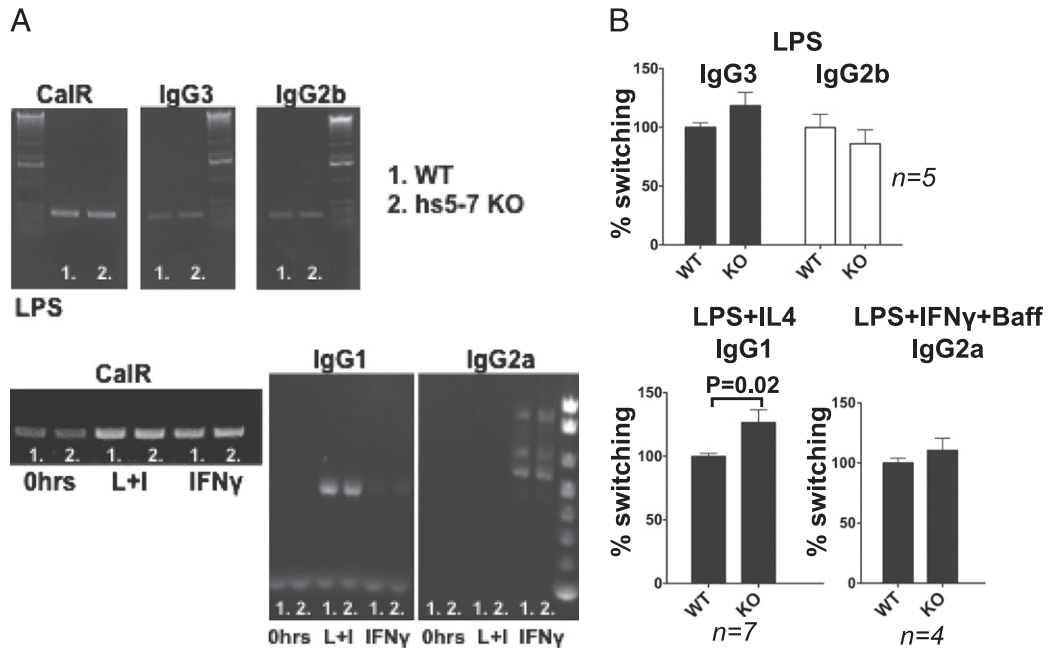
FIGURE 7. Analysis of CSR in hs5–7KO mice compared with WT mice. Splenic B cells were cultured with LPS with or without cytokines at 1×10^6 cells/ml for 48 h, at which time GT was assessed (**A**), or for 96 h, when cells were stained with anti-IgM and anti-isotype Abs to assess surface Ig expression (**B**). Experiments to measure GT were carried out in duplicate with similar results, one of which is shown. In vitro switch experiments were repeated five to seven times. Averages of WT switching were set to 100%, and hs5–7KO switching was normalized to WT amounts. CSR to IgG1 in KO mice was modestly increased relative to WT mice ($p = 0.02$, unpaired two-tailed t test). I, IL-4; IFNγ, LPS+IFNγ+Baff; L, LPS.

with an independent contribution of hs5–7 to the impact of the 3′ RR on its target sequences. It is known that switching to IgG1 is less exclusively dependent on 3′ RR enhancers than switch-

ing to other isotypes, suggesting that hs5–7's effect may be through Eμ, which has been implicated in IgG1 switching (25, 57).

FIGURE 8. 3C assays performed in B cells from WT and hs5–7KO mice analyzing interactions involving the 3′ RR and hs5–7. Physical interactions between 3′ RR enhancers and Eμ (**A**) or the J_H3 gene segment (**B**) in resting B cells of WT and hs5–7KO mice. T cells were used as a negative control. 3C assays in switching cells showed that deletion of hs5–7 does not alter interactions between the 3′ RR and I regions (**C**), or with Eμ (**D**) or between individual 3′ RR elements (**E**). These experiments show that interactions among the 3′ RR elements are detected in resting B cells and maintained at 48 h after stimulation with LPS+/− IL-4. Deletion of hs5–7 does not alter interactions or create new interactions to the nearest downstream, non-*Igh* gene, *Hole* (E).
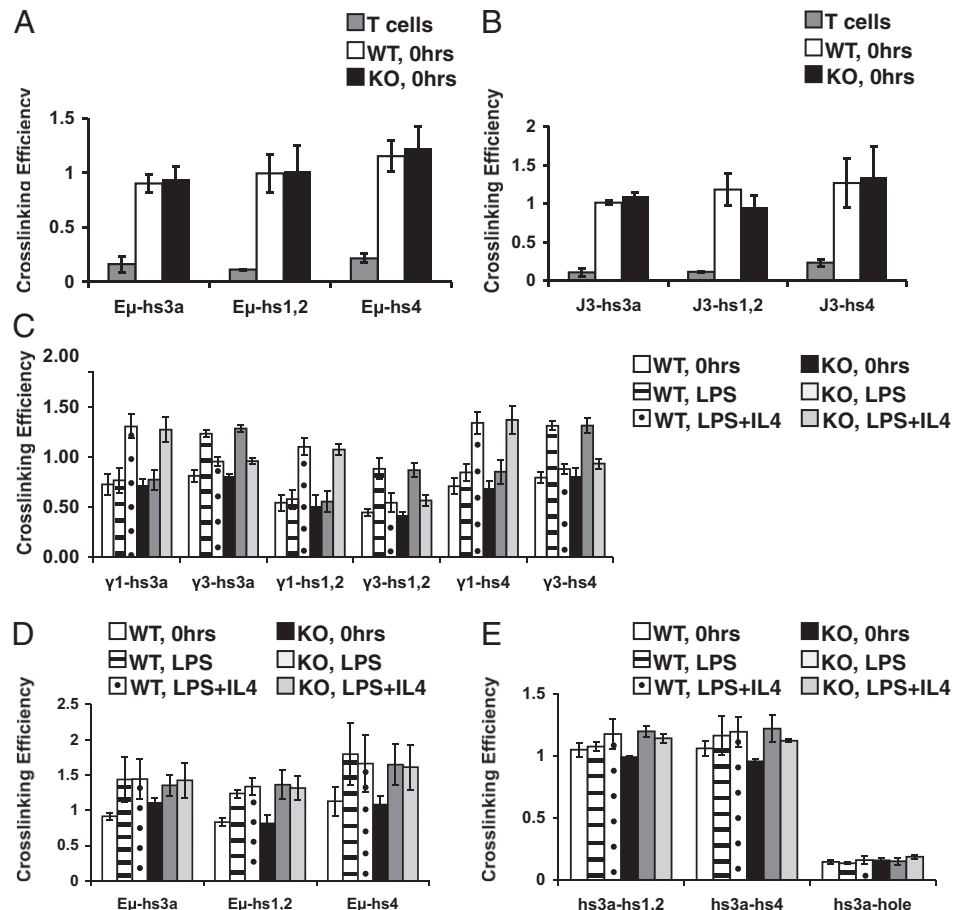
Effect of hs5–7 on VDJ rearrangement

CTCF binding sites particular to hs5–7 predict an independent role for this region in *Igh* regulation. Participation of 3′ RR elements, such as hs5–7, in VDJ rearrangement was anticipated by experiments showing that sequences downstream of the Neo insertion in Eμ KO mice might, if not blocked by Neo expression, impinge on VDJ recombination (4). Although individual or combined KOs of 3′ RR enhancers have not revealed any influence on VDJ joining (reviewed in Ref. 22), pro-B cells from hs5–7KO mice showed a reduction in V_H locus contraction and an increase in usage of proximal $V_H 7183$ genes, but not distal $V_H J558$ genes, in VDJ rearrangement. These effects likely reflect CTCF-mediated interactions between hs5–7 and target sites upstream of DFL16.1 or with V_H genes. Interactions between the 3′ RR/CTCF and DFL/CTCF sites form a loop in pre–pro-B cells that is maintained, although to a lesser extent, in pro-B cells (35) [and confirmed recently (37)]. This loop forms a domain in which D and J genes and both enhancer regions (i.e., Eμ and the 3′ RR) are located. In pro-B cells from hs5–7KO mice, 3C interactions between residual sequences in hs5 and DFL/CTCF sites are reduced. While this manuscript was being submitted for publication, a report was published describing mice in which the CTCF sites in DFL/CTCF were mutated (38). The DFL/CTCF-deleted/mutated mice showed increased rearrangement of proximal $V_H 7183$ genes, as also detected in hs5–7KO mice, as well as a decrease in the rearrangement of distal V_H genes. Thus, DFL/CTCF sites may have a more profound effect on distal V_H rearrangement than does the 3′ RR hs5–7, perhaps by direct interaction with some of the CTCF sites within the V_H locus (38). Indeed, trilateralization studies demonstrated that DFL/CTCF, located near probe h5 (39), moves into close spatial proximity with V_H genes in pro-B cells and may be pivotal for distal V_H rearrangements. Interestingly, increased rearrangement of proximal Vκ genes was detected when the Sis regulatory element, containing both CTCF and Ikaros sites, was deleted from the Vκ-Jκ intervening region (58). B cell-specific deletion of CTCF using *mb-1* Cre (59) revealed a severe developmental block at the pre-B cell stage, which was overcome substantially by introduction of a VDJ rearranged transgenic H chain gene. VDJ joining involving both distal and proximal endogenous V_H genes occurred, albeit perhaps favoring proximal genes, even though CTCF was deleted. However, the Igκ locus showed an increase in transcription of, and recombination to, proximal Vκ genes. Hence, CTCF deletion had a similar effect on Vκ gene usage (59) as did the Sis KO (58).

Although knockdown of CTCF greatly reduced the interaction of 3′ RR/CTCF with CTCF/DFL, Eμ-DFL/CTCF interactions were only modestly decreased. We propose that the hs5–7KO would maintain the Eμ-DFL loop, perhaps with Eμ in a more accessible conformation. Such a loop may preferentially aid recombination of the more proximal V_H genes, possibly involving interaction with CTCF sites in this vicinity. Notably, both CTCF and Pax5 have been implicated in *Igh* locus contraction (35, 40, 60).

Collectively, these observations suggest that hs5–7 normally contributes to a platform on which the V_H locus contracts, helping to prevent contraction and distal V_H gene rearrangement until DJ rearrangement is complete. We predict that loosened regulation between contraction and VDJ joining in the hs5–7KO pro-B cells enables a head start to proximal VDJ joining, accounting for its 2-fold increase in recombination. It will be of interest to determine the effect of this on the immune repertoire of hs5–7KO mice.

It should be noted that, in general, the hs5–7 deletion does not influence the development of hematopoietic stem cells or lymphoid tissue or B cells, and IgM expression and allelic exclusion are normal. In particular, we have not noted any differences in IgM allelic regulation in heterozygous mice. However, there are likely to be surprises in the way in which the 3′ RR functions in the *Igh* locus. For example, we observed a mild increase in DQ52-$J_H 3$ joins in hs5–7KO BM cells. This raises the question of whether a block occurs at this stage, which is ordinarily surmounted by hs5–7 activity. Of interest is that the deletion of the DQ52 promoter was associated with a decrease in usage, specifically of $J_H 3$ and other downstream Js, together with Ds upstream of DQ52, again suggestive of a regulated step of DQ52 joining (61). Both findings can be considered on the basis of interactions between hs5–7 and sites that influence use of DQ52 (i.e., CTCF sites upstream of DFL16) or other sites associated with DQ52 (e.g., a predicted Pax5 site) (61). Furthermore, other investigators described H chain allele interactions during VDJ joining (62) and interaction, via transvection, between the H chain alleles that involves CTCF binding in the 3′ RR (63). We propose that the CTCF-rich region in hs5–7 could be involved in these *cis* and *trans* interactions. Interestingly, to form translocations, dsDNA breaks generated in different loci must be juxtaposed for joining. If the CTCF sites in hs5–7 are involved in organizing distinct chromosomal territories, their removal may alter *Igh* nuclear organization and position the locus in such a way as to promote or diminish particular translocations.

CTCF sites downstream of hs5–7

Although the hs5–7 region contains a remarkably high density of CTCF (and Pax5) binding sites, in fact, significantly greater than generally seen in the genome with respect to CTCF, the phenotypic consequences of their deletion were relatively modest. Various possibilities could account for these findings. For instance, loops that involve the 3′ RR can occur, even when CTCF levels are reduced, and presumably involve other proteins (64). Candidates include YY1 (an Eμ- and 3′ RR-binding factor), which is known to affect DJ and VDJ joining (42), and cohesin, which binds to the 3′ RR in both a CTCF-dependent and -independent manner (26), and, as recently shown, affects globin gene expression (65). Eμ could also partially compensate for hs5–7 (1, 3, 4). In addition, recent ChIP-Seq data revealed that seven of nine CTCF sites downstream of hs4 were deleted in the hs5–7KO mouse (35). Two additional CTCF sites are located in the "38" region beyond the region deleted in hs5–7 (R. Casellas, personal communication) and downstream of the 50 DNA overlapping fragments analyzed by EMSA with recombinant CTCF in our original report of this genomic region (27). These residual CTCF sites could provide anchors sufficient for full levels of VDJ joining, GT, CSR, and SHM. The "38" region may have specific functions in accord with apparent independent regulation of its chromatin architecture (27).

Furthermore, CTCF sites are located in the local vicinity of each of the nearest downstream non-*Igh* genes (R. Casellas, personal communication, and J.V.-G. and A.J.F., data not shown). Although the small increase in expression of the nearest downstream non-*Igh* gene, *Hole*, in the hs5–7KO mice reveals some insulator activity of this region, it is likely that local downstream CTCF sites contribute their own insulation against inappropriate influence from upstream 3′ RR enhancers.

The experiments reported in this article show a role for the 3′ RR CTCF-rich region, hs5–7, in processes involving the *Igh* locus during B cell development. These include an impact on V_H locus contraction and VDJ rearrangement, influencing sequences located as much as 500 kb away ($V_H 7183$ family members). Although it is predicted that these processes involve CTCF, it is also likely that other proteins (64), such as Pax5, help hs5–7 to cooperate with various 3′ RR elements. It will be of interest to

identify additional interactions involving hs5–7, which may depend on CTCF or other proteins.

Disclosures

The authors have no financial conflicts of interest.

References

1. Chen, J., F. Young, A. Bottaro, V. Stewart, R. K. Smith, and F. W. Alt. 1993. Mutations of the intronic IgH enhancer and its flanking sequences differentially affect accessibility of the JH locus. *EMBO J.* 12: 4635–4645.
2. Sakai, E., A. Bottaro, L. Davidson, B. P. Sleckman, and F. W. Alt. 1999. Recombination and transcription of the endogenous Ig heavy chain locus is effected by the Ig heavy chain intronic enhancer core region in the absence of the matrix attachment regions. *Proc. Natl. Acad. Sci. USA* 96: 1526–1531.
3. Serwe, M., and F. Sablitzky. 1993. V(D)J recombination in B cells is impaired but not blocked by targeted deletion of the immunoglobulin heavy chain intron enhancer. *EMBO J.* 12: 2321–2327.
4. Perlot, T., F. W. Alt, C. H. Bassing, H. Suh, and E. Pinaud. 2005. Elucidation of IgH intronic enhancer functions via germ-line deletion. *Proc. Natl. Acad. Sci. USA* 102: 14362–14367.
5. Afshar, R., S. Pierce, D. J. Bolland, A. Corcoran, and E. M. Oltz. 2006. Regulation of IgH gene assembly: role of the intronic enhancer and 5′DQ52 region in targeting DHJH recombination. *J. Immunol.* 176: 2439–2447.
6. Li, F., and L. A. Eckhardt. 2009. A role for the IgH intronic enhancer E mu in enforcing allelic exclusion. *J. Exp. Med.* 206: 153–165.
7. Alt, F. W., N. Rosenberg, R. J. Casanova, E. Thomas, and D. Baltimore. 1982. Immunoglobulin heavy-chain expression and class switching in a murine leukaemia cell line. *Nature* 296: 325–331.
8. Burrows, P. D., G. B. Beck-Engeser, and M. R. Wabl. 1983. Immunoglobulin heavy-chain class switching in a pre-B cell line is accompanied by DNA rearrangement. *Nature* 306: 243–246.
9. Eckhardt, L. A., and B. K. Birshtein. 1985. Independent immunoglobulin class-switch events occurring in a single myeloma cell line. *Mol. Cell. Biol.* 5: 856–868.
10. Klein, S., F. Sablitzky, and A. Radbruch. 1984. Deletion of the IgH enhancer does not reduce immunoglobulin heavy chain production of a hybridoma IgD class switch variant. *EMBO J.* 3: 2473–2476.
11. Zaller, D. M., and L. A. Eckhardt. 1985. Deletion of a B-cell-specific enhancer affects transfected, but not endogenous, immunoglobulin heavy-chain gene expression. *Proc. Natl. Acad. Sci. USA* 82: 5088–5092.
12. Lieberson, R., J. Ong, X. Shi, and L. A. Eckhardt. 1995. Immunoglobulin gene transcription ceases upon deletion of a distant enhancer. *EMBO J.* 14: 6229–6238.
13. Matthias, P., and D. Baltimore. 1993. The immunoglobulin heavy chain locus contains another B-cell-specific 3′ enhancer close to the alpha constant region. *Mol. Cell. Biol.* 13: 1547–1553.
14. Madisen, L., and M. Groudine. 1994. Identification of a locus control region in the immunoglobulin heavy-chain locus that deregulates c-myc expression in plasmacytoma and Burkitt's lymphoma cells. *Genes Dev.* 8: 2212–2226.
15. Michaelson, J. S., S. L. Giannini, and B. K. Birshtein. 1995. Identification of 3′ alpha-hs4, a novel Ig heavy chain enhancer element regulated at multiple stages of B cell differentiation. *Nucleic Acids Res.* 23: 975–981.
16. Gregor, P. D., and S. L. Morrison. 1986. Myeloma mutant with a novel 3′ flanking region: loss of normal sequence and insertion of repetitive elements leads to decreased transcription but normal processing of the alpha heavy-chain gene products. *Mol. Cell. Biol.* 6: 1903–1916.
17. Dunnick, W. A., J. Shi, K. A. Graves, and J. T. Collins. 2005. The 3′ end of the heavy chain constant region locus enhances germline transcription and switch recombination of the four gamma genes. *J. Exp. Med.* 201: 1459–1466.
18. Shi, X., and L. A. Eckhardt. 2001. Deletional analyses reveal an essential role for the hs3b/hs4 IgH 3′ enhancer pair in an Ig-secreting but not an earlier-stage B cell line. *Int. Immunol.* 13: 1003–1012.
19. Pinaud, E., A. A. Khamlichi, C. Le Morvan, M. Drouet, V. Nalesso, M. Le Bert, and M. Cogné. 2001. Localization of the 3′ IgH locus elements that effect long-distance regulation of class switch recombination. *Immunity* 15: 187–199.
20. Vincent-Fabert, C., R. Fiancette, E. Pinaud, V. Truffinet, N. Cogné, M. Cogné, and Y. Denizot. 2010. Genomic deletion of the whole IgH 3′ regulatory region (hs3a, hs1,2, hs3b, and hs4) dramatically affects class switch recombination and Ig secretion to all isotypes. *Blood* 116: 1895–1898.
21. Dunnick, W. A., J. T. Collins, J. Shi, G. Westfield, C. Fontaine, P. Hakimpour, and F. N. Papavasiliou. 2009. Switch recombination and somatic hypermutation are controlled by the heavy chain 3′ enhancer region. *J. Exp. Med.* 206: 2613–2623.
22. Pinaud, E., M. Marquet, R. Fiancette, S. Péron, C. Vincent-Fabert, Y. Denizot, and M. Cogné. 2011. The IgH locus 3′ regulatory region: pulling the strings from behind. *Adv. Immunol.* 110: 27–70.
23. Yan, Y., J. Pieretti, Z. Ju, S. Wei, J. R. Christin, F. Bah, B. K. Birshtein, and L. A. Eckhardt. 2011. Homologous elements hs3a and hs3b in the 3′ regulatory region of the murine immunoglobulin heavy chain (Igh) locus are both dispensable for class-switch recombination. *J. Biol. Chem.* 286: 27123–27131.
24. Ju, Z., S. A. Volpi, R. Hassan, N. Martinez, S. L. Giannini, T. Gold, and B. K. Birshtein. 2007. Evidence for physical interaction between the immunoglobulin heavy chain variable region and the 3′ regulatory region. *J. Biol. Chem.* 282: 35169–35178.
25. Wuerffel, R., L. Wang, F. Grigera, J. Manis, E. Selsing, T. Perlot, F. W. Alt, M. Cogne, E. Pinaud, and A. L. Kenter. 2007. S-S synapsis during class switch recombination is promoted by distantly located transcriptional elements and activation-induced deaminase. *Immunity* 27: 711–722.
26. Chatterjee, S., Z. Ju, R. Hassan, S. A. Volpi, A. V. Emelyanov, and B. K. Birshtein. 2011. Dynamic changes in binding of immunoglobulin heavy chain 3′ regulatory region to protein factors during class switching. *J. Biol. Chem.* 286: 29303–29312.
27. Garrett, F. E., A. V. Emelyanov, M. A. Sepulveda, P. Flanagan, S. Volpi, F. Li, D. Loukinov, L. A. Eckhardt, V. V. Lobanenkov, and B. K. Birshtein. 2005. Chromatin architecture near a potential 3′ end of the Igh locus involves modular regulation of histone modifications during B-Cell development and in vivo occupancy at CTCF sites. *Mol. Cell. Biol.* 25: 1511–1525.
28. Yusufzai, T. M., H. Tagami, Y. Nakatani, and G. Felsenfeld. 2004. CTCF tethers an insulator to subnuclear sites, suggesting shared insulator mechanisms across species. *Mol. Cell* 13: 291–298.
29. Hou, C., H. Zhao, K. Tanimoto, and A. Dean. 2008. CTCF-dependent enhancer-blocking by alternative chromatin loop formation. *Proc. Natl. Acad. Sci. USA* 105: 20398–20403.
30. Ling, J. Q., T. Li, J. F. Hu, T. H. Vu, H. L. Chen, X. W. Qiu, A. M. Cherry, and A. R. Hoffman. 2006. CTCF mediates interchromosomal colocalization between Igf2/H19 and Wsb1/Nf1. *Science* 312: 269–272.
31. Splinter, E., H. Heath, J. Kooren, R. J. Palstra, P. Klous, F. Grosveld, N. Galjart, and W. de Laat. 2006. CTCF mediates long-range chromatin looping and local histone modification in the beta-globin locus. *Genes Dev.* 20: 2349–2354.
32. Majumder, P., J. A. Gomez, and J. M. Boss. 2006. The human major histocompatibility complex class II HLA-DRB1 and HLA-DQA1 genes are separated by a CTCF-binding enhancer-blocking element. *J. Biol. Chem.* 281: 18435–18443.
33. Degner, S. C., T. P. Wong, G. Jankevicius, and A. J. Feeney. 2009. Cutting edge: developmental stage-specific recruitment of cohesin to CTCF sites throughout immunoglobulin loci during B lymphocyte development. *J. Immunol.* 182: 44–48.
34. Featherstone, K., A. L. Wood, A. J. Bowen, and A. E. Corcoran. 2010. The mouse immunoglobulin heavy chain V-D intergenic sequence contains insulators that may regulate ordered V(D)J recombination. *J. Biol. Chem.* 285: 9327–9338.
35. Degner, S. C., J. Verma-Gaur, T. P. Wong, C. Bossen, A. M. Iverson, A. Torkamani, C. Vettermann, Y. C. Lin, Z. Ju, D. Schulz, et al. 2011. CCCTC-binding factor (CTCF) and cohesin influence the genomic architecture of the Igh locus and antisense transcription in pro-B cells. *Proc. Natl. Acad. Sci. USA* 108: 9566–9571.
36. Ebert, A., S. McManus, H. Tagoh, J. Medvedovic, G. Salvagiotto, M. Novatchkova, I. Tamir, A. Sommer, M. Jaritz, and M. Busslinger. 2011. The distal V(H) gene cluster of the Igh locus contains distinct regulatory elements with Pax5 transcription factor-dependent activity in pro-B cells. *Immunity* 34: 175–187.
37. Guo, C., T. Gerasimova, H. Hao, I. Ivanova, T. Chakraborty, R. Selimyan, E. M. Oltz, and R. Sen. 2011. Two forms of loops generate the chromatin conformation of the immunoglobulin heavy-chain gene locus. *Cell* 147: 332–343.
38. Guo, C., H. S. Yoon, A. Franklin, S. Jain, A. Ebert, H. L. Cheng, E. Hansen, O. Despo, C. Bossen, C. Vettermann, et al. 2011. CTCF-binding elements mediate control of V(D)J recombination. *Nature* 477: 424–430.
39. Jhunjhunwala, S., M. C. van Zelm, M. M. Peak, S. Cutchin, R. Riblet, J. J. van Dongen, F. G. Grosveld, T. A. Knoch, and C. Murre. 2008. The 3D structure of the immunoglobulin heavy-chain locus: implications for long-range genomic interactions. *Cell* 133: 265–279.
40. Fuxa, M., J. Skok, A. Souabni, G. Salvagiotto, E. Roldan, and M. Busslinger. 2004. Pax5 induces V-to-DJ rearrangements and locus contraction of the immunoglobulin heavy-chain gene. *Genes Dev.* 18: 411–422.
41. Su, I. H., A. Basavaraj, A. N. Krutchinsky, O. Hobert, A. Ullrich, B. T. Chait, and A. Tarakhovsky. 2003. Ezh2 controls B cell development through histone H3 methylation and Igh rearrangement. *Nat. Immunol.* 4: 124–131.
42. Liu, H., M. Schmidt-Supprian, Y. Shi, E. Hobeika, N. Barteneva, H. Jumaa, R. Pelanda, M. Reth, J. Skok, K. Rajewsky, and Y. Shi. 2007. Yin Yang 1 is a critical regulator of B-cell development. *Genes Dev.* 21: 1179–1189.

43. Reynaud, D., I. A. Demarco, K. L. Reddy, H. Schjerven, E. Bertolino, Z. Chen, S. T. Smale, S. Winandy, and H. Singh. 2008. Regulation of B cell fate commitment and immunoglobulin heavy-chain gene rearrangements by Ikaros. *Nat. Immunol.* 9: 927–936.

44. Ioffe, E., Y. Liu, M. Bhaumik, F. Poirier, S. M. Factor, and P. Stanley. 1995. WW6: an embryonic stem cell line with an inert genetic marker that can be traced in chimeras. *Proc. Natl. Acad. Sci. USA* 92: 7357–7361.

45. Kaminski, D. A., and J. Stavnezer. 2007. Antibody class switching differs among SJL, C57BL/6 and 129 mice. *Int. Immunol.* 19: 545–556.

46. Sayegh, C. E., S. Jhunjhunwala, R. Riblet, and C. Murre. 2005. Visualization of looping involving the immunoglobulin heavy-chain locus in developing B cells. [Published erratum appears in 2008 *Genes Dev.* 22: 1717.] *Genes Dev.* 19: 322–327.

47. Muramatsu, M., K. Kinoshita, S. Fagarasan, S. Yamada, Y. Shinkai, and T. Honjo. 2000. Class switch recombination and hypermutation require activation-induced cytidine deaminase (AID), a potential RNA editing enzyme. *Cell* 102: 553–563.

48. Sepulveda, M. A., F. E. Garrett, A. Price-Whelan, and B. K. Birshtein. 2005. Comparative analysis of human and mouse 3′ Igh regulatory regions identifies distinctive structural features. *Mol. Immunol.* 42: 605–615.

49. Livak, K. J., and T. D. Schmittgen. 2001. Analysis of relative gene expression data using real-time quantitative PCR and the 2(−Delta Delta C(T)) Method. *Methods* 25: 402–408.

50. Li, Z., C. Zhao, M. D. Iglesias-Ussel, Z. Polonskaya, M. Zhuang, G. Yang, Z. Luo, W. Edelmann, and M. D. Scharff. 2006. The mismatch repair protein Msh6 influences the in vivo AID targeting to the Ig locus. *Immunity* 24: 393–403.

51. Chahwan, R., S. N. Wontakal, and S. Roa. 2010. Crosstalk between genetic and epigenetic information through cytosine deamination. *Trends Genet.* 26: 443–448.

52. Maccarthy, T., S. Roa, M. D. Scharff, and A. Bergman. 2009. SHMTool: a webserver for comparative analysis of somatic hypermutation datasets. *DNA Repair (Amst.)* 8: 137–141.

53. Steele, E. J. 2009. Mechanism of somatic hypermutation: critical analysis of strand biased mutation signatures at A:T and G:C base pairs. *Mol. Immunol.* 46: 305–320.

54. Dong, C., U. A. Temann, and R. A. Flavell. 2001. Cutting edge: critical role of inducible costimulator in germinal center reactions. *J. Immunol.* 166: 3659–3662.

55. Lebecque, S. G., and P. J. Gearhart. 1990. Boundaries of somatic mutation in rearranged immunoglobulin genes: 5′ boundary is near the promoter, and 3′ boundary is approximately 1 kb from V(D)J gene. *J. Exp. Med.* 172: 1717–1727.

56. Dunnick, W. A., J. Shi, J. M. Zerbato, C. A. Fontaine, and J. T. Collins. 2011. Enhancement of antibody class-switch recombination by the cumulative activity of four separate elements. *J. Immunol.* 187: 4733–4743.

57. Cogné, M., R. Lansford, A. Bottaro, J. Zhang, J. Gorman, F. Young, H. L. Cheng, and F. W. Alt. 1994. A class switch control region at the 3′ end of the immunoglobulin heavy chain locus. *Cell* 77: 737–747.

58. Xiang, Y., X. Zhou, S. L. Hewitt, J. A. Skok, and W. T. Garrard. 2011. A multifunctional element in the mouse Igκ locus that specifies repertoire and Ig loci subnuclear location. *J. Immunol.* 186: 5356–5366.

59. Ribeiro de Almeida, C., R. Stadhouders, M. J. de Bruijn, I. M. Bergen, S. Thongjuea, B. Lenhard, W. van Ijcken, F. Grosveld, N. Galjart, E. Soler, and R. W. Hendriks. 2011. The DNA-binding protein CTCF limits proximal Vκ recombination and restricts κ enhancer interactions to the immunoglobulin κ light chain locus. *Immunity* 35: 501–513.

60. Degner-Leisso, S. C., and A. J. Feeney. 2010. Epigenetic and 3-dimensional regulation of V(D)J rearrangement of immunoglobulin genes. *Semin. Immunol.* 22: 346–352.

61. Nitschke, L., J. Kestler, T. Tallone, S. Pelkonen, and J. Pelkonen. 2001. Deletion of the DQ52 element within the Ig heavy chain locus leads to a selective reduction in VDJ recombination and altered D gene usage. *J. Immunol.* 166: 2540–2552.

62. Hewitt, S. L., B. Yin, Y. Ji, J. Chaumeil, K. Marszalek, J. Tenthorey, G. Salvagiotto, N. Steinel, L. B. Ramsey, J. Ghysdael, et al. 2009. RAG-1 and ATM coordinate monoallelic recombination and nuclear positioning of immunoglobulin loci. *Nat. Immunol.* 10: 655–664.

63. Liu, H., J. Huang, J. Wang, S. Jiang, A. S. Bailey, D. C. Goldman, M. Welcker, V. Bedell, M. L. Slovak, B. Clurman, et al. 2008. Transvection mediated by the translocated cyclin D1 locus in mantle cell lymphoma. *J. Exp. Med.* 205: 1843–1858.

64. Ju, Z., S. Chatterjee, and B. K. Birshtein. 2011. Interaction between the immunoglobulin heavy chain 3′ regulatory region and the IgH transcription unit during B cell differentiation. *Mol. Immunol.* 49: 297–303.

65. Chien, R., W. Zeng, S. Kawauchi, M. A. Bender, R. Santos, H. C. Gregson, J. A. Schmiesing, D. A. Newkirk, X. Kong, A. R. Ball, Jr., et al. 2011. Cohesin mediates chromatin interactions that regulate mammalian β-globin expression. *J. Biol. Chem.* 286: 17870–17878.

66. Zhou, J., N. Ashouian, M. Delepine, F. Matsuda, C. Chevillard, R. Riblet, C. L. Schildkraut, and B. K. Birshtein. 2002. The origin of a developmentally regulated Igh replicon is located near the border of regulatory domains for Igh replication and expression. *Proc. Natl. Acad. Sci. USA* 99: 13693–13698.